Earth and Planetary Science Letters, 117 (1993) 125–145
Elsevier Science Publishers B.V., Amsterdam

[UC]

Lanthanide and actinide chemistry at high C/O ratios in the solar nebula

Katharina Lodders [a] [1] and Bruce Fegley, Jr. [b]

[a] *CRD and C, P.O. Box 4182, Chesterfield, MO 63006, USA*
[b] *Department of Earth and Planetary Sciences and McDonnell Center for the Space Sciences, Washington University, Campus Box 1169, St. Louis, MO 63130-4899, USA*

Received June 25, 1992; revision accepted March 17, 1993

ABSTRACT

Chemical equilibrium calculations were performed to study the condensation chemistry of the REE and actinides under the highly reducing conditions which are necessary for the formation of the enstatite chondrites [1,2]. Our calculations confirm that the REE and actinides condensed into oldhamite (CaS), the major REE and actinide host phase in enstatite chondrites, at a carbon–oxygen (C/O) ratio $\geqslant 1$ in an otherwise solar gas. Five basic types of REE abundance patterns, several of which are analogous to REE abundance patterns observed in the Ca, Al-rich inclusions (CAIs) in carbonaceous chondrites, are predicted to occur in meteoritic oldhamites. All of the reported REE patterns in oldhamites in enstatite chondrites can be interpreted in terms of our condensation calculations. The observed patterns fall into 3 of the 5 predicted categories. The reported Th and U enrichments and ratios in meteoritic oldhamites are also consistent with predictions of the condensation calculations. Finally, pure REE sulfides are predicted to condense in the 10^{-6} to 10^{-9} bar range and may be found in enstatite chondrites if they formed in this pressure range.

Introduction

Oldhamite (CaS) and the other unusual refractory minerals (e.g., osbornite, TiN; niningerite, MgS; alabandite, MnS) found in the highly reduced enstatite chondrites are generally believed to be analogs to the more oxidized refractory minerals such as perovskite ($CaTiO_3$), hibonite ($CaAl_{12}O_{19}$), melilite ($Ca_2Al_2SiO_7$–$Ca_2MgSi_2O_7$), and spinel ($MgAl_2O_4$) which occur in the Ca, Al-rich inclusions (CAIs) in carbonaceous chondrites [2]. Condensation calculations by Larimer et al. [1–3] demonstrated that CaS, TiN, MgS, etc. are unstable in a solar composition gas and only become stable under more reducing conditions characterized by higher carbon–oxygen (C/O) ratios in the gas. Conversely, the more oxidized minerals found in the CAIs are unstable under these more reducing conditions and their places in the condensation sequence are assumed by phases such as CaS, MgS and TiN.

Numerous studies of the trace element chemistry of perovskite and hibonite, two major REE host phases in CAIs, have provided important information on the origin of CAIs and on chemical and physical conditions in the solar nebula [e.g., 4, 5, and references therein]. Therefore, it is reasonable to expect that studies of the trace element composition of CaS and the other unusual minerals in enstatite chondrites will prove similarly informative. Indeed selective dissolution experiments on bulk samples, analyses of meteorite fragments with different abundances of CaS and other minerals, and fission track radiography suggest that CaS is an important host phase for the REE and actinides in enstatite chondrites [6–8]. Recently several groups published results

[1] Present address: Department of Earth and Planetary Sciences, Washington University, Campus Box 1169, St. Louis, MO 63130-4899, USA.

of trace element analyses of CaS and other phases in enstatite chondrites which clearly demonstrate that oldhamite is the major carrier of the REE and actinides in these meteorites. These studies also show that secondary minerals such as phosphates, which are REE and actinide host phases formed during metamorphism of ordinary chondrites, are not important REE host phases in the enstatite chondrites. The absence of such phases (or their very low abundance) suggests that metamorphism has not significantly altered the REE and actinide abundance patterns. An additional argument suggesting that metamorphism has not altered the REE and actinide abundances in oldhamite is that metamorphic equilibration temperatures for the CaS–enstatite cosmothermometer do not correlate with the petrologic grade of EH and EL chondrites [9, and references therein]. The lack of correlation suggests that the CaS in the primitive E-chondrites was not affected by metamorphism and thus it is reasonable to assume that the trace elements contained in the CaS were also unaffected.

Larimer and Ganapathy [10,11] used neutron activation to make the first analyses of oldhamite, sinoite (Si_2N_2O), and osbornite from different meteorites. They found large enrichments of the REE in oldhamite from Indarch (EH4) and Yilmia (EL6) but only low levels of the REE in osbornite and sinoite from Yilmia. They argued persuasively that nebular condensation of the REE into oldhamite is the most likely way to explain the large REE enrichments. Subsequently, Lundberg et al. made ion microprobe analyses of oldhamite and niningerite from several enstatite chondrites [12,13]. This work confirmed that CaS is the major host for the REE, showed the existence of several different types of REE patterns, and also showed that some oldhamites were isotopically anomalous and had small deficits in ^{48}Ca. Murrell and Burnett [14] showed that Th and U generally are also concentrated in oldhamite, although niningerite is a minor carrier for U in one sample of Abee (EH4).

Condensation calculations at high C/O ratios are necessary in order to interpret the observed REE patterns and actinide abundances in terms of nebular and/or parent body processes. However, prior results [15–17] are mainly qualitative and only indicate that REE condensation into oldhamite may occur. Here we present detailed REE and actinide condensation calculations which provide information on the gas phase chemistry of the REE and actinides, on their condensation chemistry, and predict specific REE and actinide abundance patterns in CaS formed under these conditions. We also compare the observed REE patterns with our predictions and show how the observations can be interpreted in terms of condensation from an otherwise solar gas with a C/O ratio $\geqslant 1$. Finally, we present arguments indicating that the REE-rich oldhamites found in enstatite chondrites are nebular condensates.

Method of calculation

The condensation calculations were performed using a new computer code named CONDOR, which calculates gas–solid chemical equilibrium as a function of temperature, pressure, and elemental abundances. The computation procedure is similar to that used in the TOP20 [18] and METKON [4,19] codes. Briefly, CONDOR calculates the molecular distribution of an element by considering all gases of that element for which thermodynamic data are available. For example, in the case of Ce, the total abundance of Ce in all forms is defined as $A(\mathrm{Ce})$, which is simply the solar abundance of Ce [20]. The mole fraction of total Ce is then:

$$X_{\Sigma \mathrm{Ce}} = A(\mathrm{Ce})/A(\mathrm{H} + \mathrm{H_2} + \mathrm{He}) \qquad (1)$$

where $A(\mathrm{H} + \mathrm{H_2} + \mathrm{He})$ is the sum of the solar abundances of H, and He (considering the temperature-dependent H and H_2 equilibrium). Multiplying $X_{\Sigma \mathrm{Ce}}$ by the total pressure P_T gives the total pressure of Ce in all forms, which is equivalent to the partial pressure sum for Ce:

$$P_{\Sigma \mathrm{Ce}} = X_{\Sigma \mathrm{Ce}} P_T = P_{\mathrm{Ce}} + P_{\mathrm{CeO}} + P_{\mathrm{CeO_2}} + P_{\mathrm{CeS}} + \ldots \qquad (2)$$

where P_i is the partial pressure of gas i. This expression can be rewritten in terms of the thermodynamic activity of Ce (a_{Ce}), the equilibrium constants (K_i) for forming the different gases from the constituent elements in their reference states, and the thermodynamic activities and fu-

gacities of the other elements combined with Ce in these gases:

$$P_{\Sigma Ce} = X_{\Sigma Ce} P_T = a_{Ce}\left[K_{Ce} + K_{CeO}(f_{O_2})^{1/2} + K_{CeO_2}(f_{O_2}) + K_{CeS}(f_{S_2})^{1/2} + \ldots\right] \quad (3)$$

One such equation is written for each element in the code.

The equilibrium constants K_i in these equations are taken from different thermodynamic data sources in the literature (described below). An initial guess is assumed for the activity (or fugacity) of each element. The guesses can be optimized if the major gas of each element is known, but this is not necessary for the code to operate properly. The CONDOR code then solves the set of coupled nonlinear equations and gives the thermodynamic activity (or fugacity) for each element, the abundances of all gases in the code, and information on the quality of the solution for each element. The code reaches a solution when the calculated abundance and the input abundance for each element agree within 1 part in 100,000 to insure that mass balance is achieved. At present, 56 elements (H, Na, K, Mg, Ca, Sr, Ba, Sc, Y, Ti, Zr, Hf, V, Nb, Ta, Cr, Mo, W, Mn, Fe, Co, Ni, Cu, Zn, Al, C, Si, N, P, O, S, F, Cl, Br, REE, Th, U, Pu, noble gases) and ~600 gases are included in CONDOR. In some cases (e.g., yttrium) data are available for gases but not for potentially important condensates at high C/O ratios. Here we focus on the REE and the actinides. However, the entire set of elements and compounds was included in the calculations.

CONDOR calculates the thermodynamic activities of a large number of possible condensates by considering the formation reactions from the constituent elements in their respective reference states. For example, in the case of Ce, CONDOR calculates the activities of CeO_2(s), Ce_2O_3(s), CeC_2(s), CeN(s), and CeS(s) from the equations:

$$a_{CeO_2} = (a_{Ce})(f_{O_2})K_{CeO_2} \quad (4)$$

$$a_{Ce_2O_3} = (a_{Ce})^2(f_{O_2})^{3/2}K_{Ce_2O_3} \quad (5)$$

$$a_{CeC_2} = (a_{Ce})(a_{gr})^2 K_{CeC_2} \quad (6)$$

$$a_{CeN} = (a_{Ce})(f_{N_2})^{1/2} K_{CeN} \quad (7)$$

$$a_{CeS} = (a_{Ce})(f_{S_2})^{1/2} K_{CeS} \quad (8)$$

where a_{gr} is the activity of graphite, which is the reference state for carbon.

The CONDOR program calculates the condensation of pure phases (e.g., CaS) and trace phases in solid solution (e.g., the REE and actinides). Approximately 180 condensates of major, minor, and trace elements are included in the code. Once a condensate becomes stable, the fraction (α) of the element which is condensed is calculated (assuming ideal solid solution for a trace element), and the total gas phase abundance of the element is reduced by multiplying by $(1 - \alpha)$. Because the gas phase and gas–solid equilibrium calculations are coupled, the gas phase chemistry and gas–solid condensation calculations are done simultaneously using iterative techniques, as in the METKON code [4].

The condensation calculations assume ideal solid solution because no activity coefficient data are available for the solid solutions of CaS with the sulfides considered here. However, CaS and the REE and actinide sulfides all have the NaCl crystal structure, indicating that their solid solutions will be close to ideal. For example, the calorimetric data of Charlu et al. [21] in combination with the theoretical mixing entropies of Waldbaum [22] show that the melilite solid solution, in which both endmembers have the same crystal structure, is close to ideal.

The solar elemental abundances are from Anders and Grevesse [20], except for the Pu abundance which was calculated from the $^{244}Pu/^{238}U$ ratio given by Jones [23]. We adopted a solar C/O ratio of 0.42 from Anders and Grevesse [20]. More recent work by Grevesse et al. [24] gives a slightly higher value of 0.47, while Cameron's compilations [25] gave solar C/O ratios of 0.55 (in 1973) and 0.60 (in 1982).

The carbon–oxygen (C/O) ratio was varied by either increasing the carbon abundance or decreasing the oxygen abundance. The calculations were done at a C/O ratio of 1.2 (enhanced carbon abundance), which was chosen to allow comparisons with past work [2,15–17,26] done at the same or a nearly identical C/O ratio. However, with the exception of graphite and metal carbides, the condensation sequence is independent of the C/O ratio above unity (see Discussion). The calculations were usually done from 1000 to 2000 K and covered a pressure range

from 10^{-3} to 10^{-9} bar. However, larger temperature ranges were used for calculations at very low pressures. Most of the results presented here are at 10^{-3} bar to facilitate comparisons to prior work.

Thermodynamic data sources and estimates

The thermodynamic data for gases and condensates of the elements Al, C, Ca, Cl, Co, Cr, F, Fe, H, Mg, N, Na, K, Mn, Ni, O, P, S, Si, Ti, Zn were taken from standard compilations [27–35]. All of the gases listed by Larimer and Bartholomay [2] were included as well as some others which they did not consider (Cl, F, Mn, Zn, and P gases).

Eighty five compounds were considered for the REE and actinides. These compounds and the thermodynamic data sources used are listed in Table 1. The uncertainties in the data are either taken from the references cited in Table 1, or from the original experimental papers cited in the

TABLE 1

Thermodynamic data sources for lanthanide and actinide compounds [1]

Data Source	Compounds
	Gases
Ackermann & Chandrasekharaiah [36]	UO, UO_2
Holley et al. [37]	UC_2
Murad (pers. comm..), Murad & Hildenbrand [38]	LaO, PrO, NdO, SmO, EuO, GdO, TbO, DyO, HoO, ErO, TmO, YbO, LuO
Mignanelli et al. [39]	CeO, CeO_2
Myers & Graves [40] (Gibbs free energy function)	$SmCl_3$ $\Delta H_f°(298) = -710$kJ mole^{-1} was estimated
Hultgren [29]/Pankratz [31]	La, Ce, Pr, Nd, Sm, Eu, Gd, Tb, Dy, Ho, Er, Tm, Yb, Lu, Th, ThO, ThO_2, U, Pu
Pankratz [32]	$LaCl_3$, LaF_3, $CeCl_3$, CeF_3, $PrCl_3$, PrF_3, $NdCl_3$, NdF_3, SmF_3, $EuCl_3$, EuF_3, $GdCl_3$, GdF_3, $TbCl_3$, TbF_3, $DyCl_3$, DyF_3, $HoCl_3$, HoF_3, $ErCl_3$, ErF_3, $TmCl_3$, TmF_3, $YbCl_3$, YbF_3, $LuCl_3$, LuF_3, $ThCl_4$, ThF_2, ThF_3, ThF_4, UF_4, UF_5, UF_6, PuF_6
Mills [30]/Pankratz et al. [34]	LaS, CeS, PrS, NdS, SmS, EuS, GdS, TbS, DyS, HoS, ErS, TmS, YbS, LuS, ThS, ThS_2, US, US_2
Rand [41]	ThC_2, ThC_4
	Solids
Ackermann & Chandrasekharaiah [36]	UO_2, U_2O_3
Brown & Clark [42,43]	PrN, NdN, SmN, EuN, GdN, TbN, DyN, HoN, ErN, TmN, YbN, LuN
Glusko et al. [44][$\Delta H_f°(298)$], Haschke & Deline [45] [S°(298)]	EuC_2, DyC_2, HoC_2, ErC_2, TmC_2, YbC_2, LuC_2 C_p estimated as described by Kubaschewski & Alcock [46]
Gschneidner & Kippenhan [47]	LaC_2, LaN, CeC_2, CeN, PrC_2, NdC_2, SmC_2, GdC_2
Holley et al. [37]	UC, $UC_{1.94}$, U_2C_3, $PuC_{0.84}$, Pu_2C_3
Pankratz [31]	La_2O_3, CeO_2, Pr_2O_3 Nd_2O_3, Sm_2O_3, EuO, Eu_2O_3, Gd_2O_3, Tb_2O_3, Dy_2O_3, Ho_2O_3, Er_2O_3, Tm_2O_3, Yb_2O_3, Lu_2O_3, ThO_2, PuO, PuO_2, Pu_2O_3
Pankratz et al. [33]	Th_2S_3, UN, PuN
Pankratz et al. [34]/Gronvold [48]	ThS, ThS_2, US, US_2, PuS
Rand [41]	ThC, $ThC_{1.94}$, ThN, Th_3N_4, Th_2N_2O, ThP, Th_3P_4, ThH_2
Robie et al. [35]	Ce_2O_3
see Table 2 for data and references	LaS, CeS, PrS, NdS, SmS, EuS, GdS, TbS, DyS, HoS, ErS, TmS, YbS, LuS

[1] No data are available for TbC_2(solid) and it was not included in the calculations.

Note: Compilations by Pankratz [31–34] do not list uncertainties in thermodynamic data. Uncertainties used in calculations were taken from original references cited there.

TABLE 2

Selected values of the thermodynamic properties of the rare earth and actinide monosulfide solids

	$-\Delta H°_f$(298.15K)	Ref.	S°(298.15K)	Ref.	Cp°(298.15K)	Ref.	Cp°(T) = a + b•10^{-3}T +c•10^{+5}T^{-2} (J/(mole•K), 298.15-2000K)			Ref.	T_{fus}
	kJ/mole		J/(mole•K)		J/(mole•K)		a	b	c		K
LaS	452±17	[49]	68.2±*8*	[50]	48.1	[30](a)	46.48	5.4	0	[30](a)	2600
CeS	456.5±8	[30]	78.2±1.3	[30]	49.96	[30]	42.01	26.74	0	[30]	2723
PrS	452±25	[30]	85.40±*8*	[50]	50.46	[50]	53.47	4.192	-3.807	[34]	2500
NdS	452±*63*	[51](a)	77.8±4	[30]	48.7	[30]	46.19	8	0	[30]	2400
SmS	456±*63*	[51](a)	81.2±4	[44]	58.16	[44]	*57.78*	*1.30*	*0*	(c)	2213
EuS	459.0±10.9	[52]	98.7±3.8	[53]	50	[53]	48.74	4.81	0	[53]	2673
GdS	464±17	[51]	85.06±*8*	[50]	48.1	[53]	*46.23*	*6.3*	*0*	(c)	2300
TbS	460±42	[30](a)	77.4±8	[30](a)	*50*	(b)	*48.62*	*5.40*	*0*	(c)	2240
DyS	460±63	[30](a)	77.4±8	[30](a)	*50*	(b)	*48.62*	*5.36*	*0*	(c)	2250
HoS	460±63	[30](a)	77.4±8	[30](a)	*50*	(b)	*48.66*	*5.23*	*0*	(c)	*2300*
ErS	460±63	[30](a)	77.4±10.5	[30](a)	*50*	(b)	*48.66*	*5.23*	*0*	(c)	*2300*
TmS	460±63	[30](a)	77.4±10.5	[30](a)	*50*	(b)	*48.66*	*5.23*	*0*	(c)	*2300*
YbS	452±63	[30] (a)	77.4±10.5	[30](a)	35.6	[30](a)	37.33	0.046	-1.561	[30](a)	2393
LuS	416.7±13.0	[54]	63±13	[30](a)	*50*	(b)	*48.66*	*5.23*	*0*	(c)	*2300*
ThS	399.6±4	[48]	69.79±0.33	[48]	47.74	[48]	50.12	5.460	-3.586	[48](a)	2723
US	322±13	[48]	77.99±0.21	[48]	50.54	[48]	52.857	6.515	-3.782	[48]	2753
PuS	364±38	[48](a)	76.15±8	[48](a)	48.33	[48]	45.643	14.209	-1.381	[34,48]	2623

(a) Literature value is an estimate.
(b) Cp° (298.15K) estimated as 25.1 J/(grm-atom·K) as recommended by Mills [30] and Kubaschewski and Alcock [46].
(c) Cp°(T) equation estimated from Cp° (298.15K) value and an assumed Cp° = 30.33 J/(grm-atom·K) at the sulfide melting point. A linear variation of Cp° with temperature is assumed. This method is recommended by Kubaschewski and Alcock [46].
Numbers in *italics* indicate estimates made here.

TABLE 3

Condensation temperatures of refractory minerals in a solar gas at a pressure of 10^{-3} bar

		Condensation Temperature (K)		
Mineral	Ideal Formula	This Work	Ref. [55,56]	Ref. [26,57]
Corundum	Al_2O_3	1772	1741[a]	1749[c]
Hibonite	$CaAl_{12}O_{19}$	1748	1730[a]	1725[c]
Perovskite	$CaTiO_3$	1687	1677[a]	1675[c]
Gehlenite	$Ca_2Al_2SiO_7$	1624	1608[a]	1607[c]
Spinel	$MgAl_2O_4$	1505	1488[a]	1494[c]
Iron Metal	Fe	1453	1458[b]	1458[d]
Forsterite	Mg_2SiO_4	1442	1429[b]	1433[d]

[a] Kornacki and Fegley [55].
[b] Palme and Fegley [56].
[c] Grossman et al. [57].
[d] Lattimer and Grossman [26]. [26,55–57] use abundances by Cameron [25].

compilations. The selected thermodynamic data for the solid REE and actinide monosulfides are summarized in Table 2.

The equilibrium constants used in the calculations were either taken from standard compilations or were calculated from the Gibbs energy functions and the enthalpy using the Third Law method [27]. Sometimes, the enthalpy of formation of a solid compound was known at 298 K but not the entropy. In these cases, the equilibrium constants were calculated by the Second Law method (requires an estimated entropy) or by the Third Law method (requires an estimated entropy and an estimated heat capacity). The entropy and heat capacity estimates were made using the procedures recommended by Kubaschewski and Alcock [46]. Tests made by estimating known entropies and heat capacities of solids showed that the estimates are good to within ± a few J $mole^{-1}$ K^{-1}. Thus, over the 1000 to 2000 K range, the errors introduced from the entropy and heat capacity estimates are smaller than the uncertainties in the experimentally measured enthalpies.

Results

Major element condensate

Modelling REE and actinide condensation into host phases such as perovskite and hibonite in a solar gas or into oldhamite at higher C/O ratios requires calculating the point where these host phases condense and their abundance as a function of temperature. Table 3 shows a subset of results for major element condensation at 10^{-3} bar in a solar gas. Overall, there is good agreement with previous work [e.g., 26, 55–57]. However, we calculate slightly higher condensation temperatures for oxides and silicates than reported in previous studies. This is due to using the solar C/O ratio of 0.42 from Anders and Grevesse [20] instead of the higher solar C/O ratio of about 0.6 used in the past work.

Table 4 shows an analogous comparison for major element condensation at 10^{-3} bar and at a C/O ratio of 1.2. Again, there is generally good agreement with the previous results. Our calculations at 10^{-4} bar reproduce most of the results in Larimer's calculations [1,2], which were done at this pressure. However, we calculate that TiC is the initial Ti condensate, instead of TiN. This is probably an error in the calculations of [2] because others [15,16,26] also calculate that TiC condenses first.

The results in Table 4 were calculated by increasing the carbon abundance above the solar value. The condensation temperatures of TiC, graphite, and SiC decrease to 1870, 1600, and 1723 K, respectively, if the C/O ratio is increased to 1.2 by reducing the oxygen abundance of an otherwise solar gas. If the C/O ratio is increased by removing oxygen, the condensation sequence for graphite and SiC is reversed. However, in

TABLE 4

Condensation of refractory minerals at C/O = 1.2 and 10^{-3} bar

		Condensation Temperature (K)		
Mineral	Ideal Formula	This Work	Ref. [15]	Ref. [26]
Titanium Carbide	TiC	1893	1888	1893
Graphite	C	1766[a]	1735	1732
Moissanite	SiC	1736	1740	1742
Cohenite	Fe_3C	1453	1454	1463
Aluminum Nitride	AlN	1398	1389	1396
Oldhamite	CaS[b]	1379	1313	1385
Forsterite	Mg_2SiO_4	1152	1146	1154
Osbornite	TiN	1015	1021	1025

The C/O ratio was increased by adding carbon.

[a] Graphite condenses at 1734 K if the solar abundances of Cameron [25] are used, as was done in [15,26].

[b] Sears et al. [16] condense CaS at 1377 K at 10^{-3} bar.

both cases the condensation temperatures of the other refractory condensates listed in Table 4 will be the same. This happens because once carbon is in excess the reaction $C(g) + H_2O(g) = CO(g) + H_2(g)$ fixes the H_2O/H_2 ratio. Furthermore, once graphite is condensed the carbon activity is fixed at unity and the pressure of monatomic carbon gas follows the graphite vapor pressure curve.

Another interesting point illustrated by the results in Tables 3 and 4 is that perovskite and hibonite condense about 310 to 370 K higher than oldhamite. Niningerite MgS, which conceivably could also be a host for REE and actinide sulfides, does not form until even lower temperatures of about 1030 K (at 10^{-3} bar) as a reaction product of forsterite and $H_2S(g)$. As shown in Table 5, all of the REE and actinides have completely condensed into solids by this temperature. The lower condensation point of MgS and the fact that it is formed from forsterite (which is not a favorable REE host phase) instead of as a condensate from the gas, may help to explain why in fact MgS is generally not an important REE and actinide host phase in enstatite chondrites.

Trace element gas phase chemistry

We calculated REE and actinide gas phase chemistry from 1000 to 2000 K. The results at the

TABLE 5

50% condensation temperatures (K) for the REE and actinides

Ideal Solid Solution in $CaTiO_3$ at C/O = 0.42 (solar)				Ideal Solid Solution in CaS at C/O = 1.2 (Carbon Abundance Increased)			
	$\log_{10}$ Total Pressure (Bars)				$\log_{10}$ Total Pressure (Bars)		
Oxide	-3	-6	-9	Sulfide	-3	-6	-9
$CaTiO_3$[a]	1687	1471	1303	CaS[b]	1379	1154	995
La_2O_3	1628	1413	1253	LaS	1379	1166[b]	1049[b]
Ce_2O_3	1551	1309	1130	CeS	1379	1183[b]	1057[b]
Pr_2O_3	1627	1407	1239	PrS	1379	1154	1014[b]
Nd_2O_3	1651	1430	1264	NdS	1379	1154	1013[b]
Sm_2O_3	1654	1455	1282	SmS	1368	1147	990
Eu_2O_3	1420	1249	1116	EuS	1360	1138	978
Gd_2O_3	1687	1471	1303	GdS[b]	1418	1239	1093
Tb_2O_3	1687	1471	1303	TbS	1379	1184[b]	1048[b]
Dy_2O_3	1687	1471	1303	DyS	1379	1154	995
Ho_2O_3	1687	1471	1303	HoS	1379	1154	995
Er_2O_3	1687	1471	1313[a]	ErS	1379	1154	998[b]
Tm_2O_3	1687	1471	1303	TmS	1376	1153	995
Yb_2O_3	1575	1386	1238	YbS	1268	1067	922
Lu_2O_3	1687	1471	1309[a]	Lu_2O_3[a]	1387	1194	1045
				LuS	1379	1177[b]	1043[b]
ThO_2	1687	1471	1303	ThN[c]	1481	1362	1251
UO_2	1676	1440	1271	US/UC	1379	1240[d]	1156[d]
PuO_2	1633	1435	1275	PuS	1378	1154	995

[a] Condenses as a pure oxide.
[b] Condenses as a pure sulfide.
[c] ThN condenses instead of ThS.
[d] UC condenses instead of US at these pressures.

condensation temperatures of perovskite (T_{cond} = 1687 K at 10^{-3} bar and C/O = solar), and oldhamite (T_{cond} = 1379 K at 10^{-3} bar and C/O = 1.2) are illustrated in Fig. 1. The most important gases are the elemental, oxide, and sulfide gases. Fluorides and chlorides were also considered but their abundances are many orders of magnitude below 1% of the total.

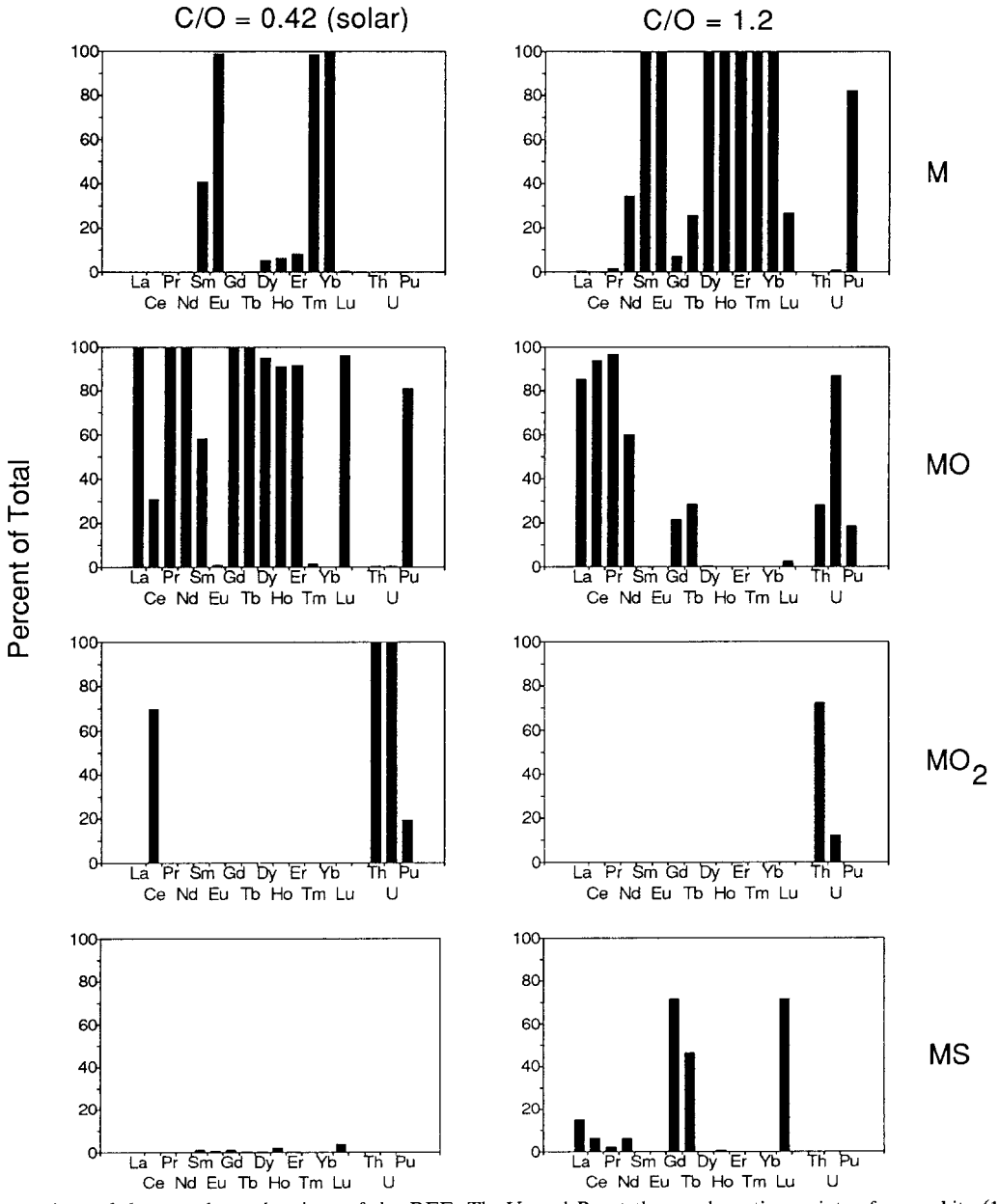

Fig. 1. A comparison of the gas phase chemistry of the REE, Th, U, and Pu at the condensation points of perovskite (1687 K, C/O = 0.42) and of oldhamite (1379 K, C/O = 1.2, carbon abundance increased) at 10^{-3} bar total pressure. The bar graphs show the percentage of an element present as elemental, monoxide, dioxide, and sulfide gases. Note that the monoxide and dioxide gases become relatively less important at C/O = 1.2 and that the elemental and sulfide gases become relatively more important at C/O = 1.2. Similar results are obtained if the REE monoxide data of Pedley and Marshall [58] are used instead of the data from [38,39].

In general the results in Fig. 1 show that the oxide gases become less important as the C/O ratio increases and that the elemental and sulfide gases become more important. Under solar conditions, at 1687 K, only Eu, Tm, and Yb are dominantly present as the elemental gases. Samarium is present as both Sm and SmO in approximately equal amounts. Otherwise the dominant gases are the monoxides. The only elements where the dioxides are the most abundant gases are Ce, Th, and U. The monosulfide gases are less important.

Under more reducing conditions (C/O = 1.2), at 1379 K, the elemental gases become more important for the heavy REE and Pu, while the monoxides are still the major gases for the light REE. In this case Ce also follows the trend of the other light REE and CeO_2(g) is unimportant. Only Th is mainly present as the dioxide gas at the oldhamite condensation temperature, whereas for U the monoxide gas becomes more stable. The monosulfide gases are the major species for Gd, Tb, and Lu. These elements are also the most refractory ones under reducing conditions (see below).

REE and actinide condensation

Table 5 shows the 50% condensation temperatures for the REE and actinides dissolved in perovskite (C/O = solar) and in oldhamite (C/O = 1.2) assuming ideal solid solution. Our perovskite condensation calculations agree with the previous results of Kornacki and Fegley [4]. The 50% condensation temperatures in Table 5 are given at 10^{-3}, 10^{-6}, and 10^{-9} bar to illustrate pressure-dependent trends.

The REE fractionate much less at high C/O ratios than under solar conditions. In a solar gas, Eu, Yb, and Ce have lower 50% condensation temperatures than the other REE. At C/O = 1.2 Eu and Yb are more volatile than the other REE including Ce. In a solar gas the LREE generally condense after the heavy REE. However, to a first approximation, at C/O = 1.2 the light and heavy REE are equally refractory with 50% condensation temperatures identical or very close to the condensation temperature of oldhamite. This trend is followed by the actinide sulfides which are also about as refractory as most of the REE.

With decreasing pressure, more pure solid REE sulfides become stable and condense prior to oldhamite (Table 5). At 10^{-3} bar pressure, only GdS condenses as a pure sulfide prior to oldhamite. At 10^{-9} bar LaS, CeS, PrS, NdS, GdS, TbS, ErS, and LuS condense prior to oldhamite. In principle, this condensation behavior could serve as a cosmobarometer for the total pressure, with the presence of sulfide grains rich in Gd, Tb, and other REE, but poor in CaS indicating formation under low nebular pressures. It is possible that the pure sulfides which condense prior to oldhamite may in fact form solid solutions with one another. The composition of these solutions has not been modelled but ideal solid solution calculations could be done if there were observations indicating the presence of ultrarefractory REE sulfide grains in enstatite chondrites.

The condensation behavior of Th, U, and Lu is slightly more complex than that predicted for the other elements. The available thermodynamic data, which are of uncertain quality for ThN and Th_2N_2O, show that ThN will be the first condensate at high C/O ratios. As shown in Table 5, at 10^{-3} bar ThN condenses about 100 K higher than oldhamite. This difference increases to about 250 K at 10^{-9} bar, but decreases to about 10 K at 10^{-2} bar. Thorium oxynitride (Th_2N_2O) and thoria (ThO_2) are also predicted to be more stable than ThS, but they are not as stable as ThN. Uranium monosulfide is the initial condensate at 10^{-3} bar but UC is predicted to be the initial condensate at lower pressures ($\leqslant 10^{-6}$ bar). Over the entire pressure range studied, Lu_2O_3 is predicted to condense a few degrees before LuS condensation into oldhamite occurs. This small difference is within the combined uncertainties of the thermodynamic data and may not be significant.

In principle, the condensation of Th as ThN and of U as either US in CaS or as UC could lead to Th/U fractionations at high C/O ratios. Any potential fractionation may be minimized by solid solution between ThN, UC, and CaS, all of which have the NaCl structure. At present not enough data on the relevant phase diagrams and on diffusion coefficients are available to make any unambiguous predictions in this area. However, at pressures of 10^{-3} to 10^{-9} bar, ThN is predicted

to condense about 100 K higher than either US dissolved in CaS or than UC. This temperature difference could lead to Th/U fractionation.

As noted above, the REE fractionate less in a gas with a high C/O ratio than in the solar gas because most of the REE and the actinides will condense into oldhamite within a few degrees of CaS condensation. With a few exceptions, any fractionation between the REE and actinides could only be produced by removing an oldhamite grain from equilibrium with the nebular gas within a very small temperature interval after it first condensed. The oldhamite grain would then be most enriched in the most refractory REE and actinides, and the remaining gas would be enriched in the less refractory REE and actinides. This postulated process is in fact analogous to the generally accepted mechanism proposed for the formation of the REE patterns observed in the ultrarefractory and the complementary Group II inclusions in CAIs [59,60]. We therefore decided to model the formation of an ultrarefractory oldhamite in a gas with a C/O ratio greater than unity.

Figure 2 and Table 6 present the results of the calculations. Figure 2 shows the fractions of the REE and actinides condensed into CaS at 1378.6 K, just 0.1 K lower than the condensation temperature of oldhamite. The uncertainties in the calculated fractions condensed are illustrated by the dashed lines. Table 6 lists the same information and also shows the corresponding gas/solid distribution coefficients (D). The D values are related to the fraction condensed (α) via the equation $D(\text{gas/solid}) = (1 - \alpha)/\alpha$.

The uncertainties in the Gibbs free energies for the solid REE and actinide monosulfides (Table 2) and for the dominant REE and actinide gases (Fig. 1) were quadratically combined in order to estimate the uncertainties for the different possible condensation reactions of the REE and actinides:

$$M(g) + H_2S(g) = MS(s) + H_2(g) \quad (9)$$

$$MO(g) + H_2S(g) = MS(s) + H_2O(g) \quad (10)$$

$$MO_2(g) + H_2S(g) + H_2(g) = MS(s) + 2H_2O(g) \quad (11)$$

$$MS(g) = MS(s) \quad (12)$$

These calculations show that the largest uncer-

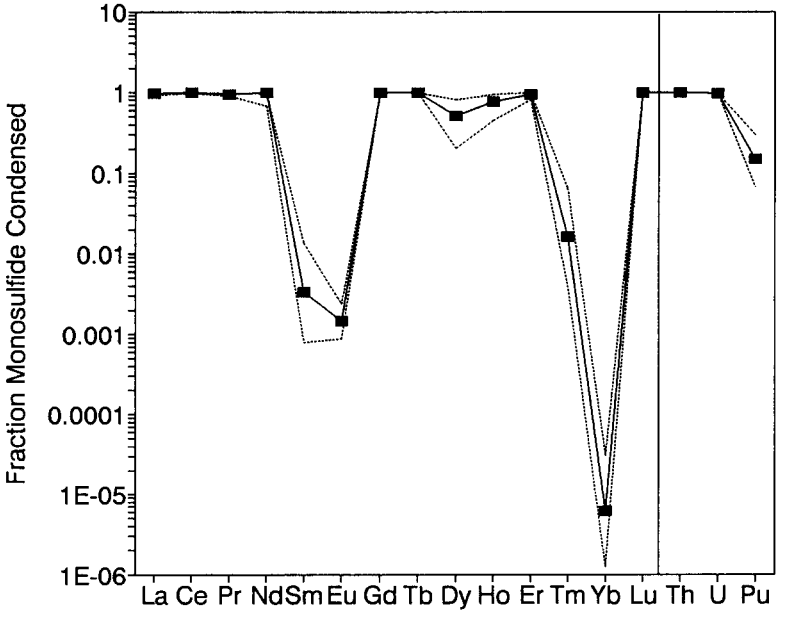

Fig. 2. The fraction of the REE and actinides which are predicted to condense into oldhamite at 1378.6 K, 0.1° below the CaS condensation point ($P = 10^{-3}$ bar, C/O = 1.2, carbon abundance increased). The dashed lines represent the range allowed by the uncertainties in the thermodynamic data in the condensation reactions (see text and Table 2). The classification for highly refractory, refractory and volatile elements derived from this graph is also given in Table 6.

TABLE 6

Percent of REE and actinide monosulfides condensed into CaS and the corresponding gas/solid distribution coefficients (D) [a]

	% Condensed	Range % Condensed[b]	D (Gas/Solid)
highly refractory			
Gd	99.96	99.91 - 99.98[c]	0.0004
Lu	99.86	99.72 - 99.93	0.0014
Tb	99.84	99.56 - 99.94	0.0016
Th	99.81	99.54 - 99.92	0.0019
refractory			
Ce	98.0	96.7 - 98.8	0.020
U	96.0	94.0 - 97.3	0.042
La	95.9	92.5 - 97.9	0.043
Pr	95.2	90.3 - 97.7	0.050
Er	94.4	80.2 - 98.6	0.059
Nd	89.2	97.1 - 67.0	0.12
Ho	77.0	44.8 - 93.3	0.30
Dy	51.5	20.4 - 81.5	0.94
volatile			
Pu	14.8	6.7 - 29.5	5.8
Tm	1.6	0.4 - 6.5	62
Sm	0.33	0.08 - 1.4	300
Eu	0.15	0.09 - 0.24	670
Yb	0.0006	0.0001 - 0.0031	166700

[a] The calculations are done at 1378.6 K, 0.1 K below the oldhamite condensation point ($P = 10^{-3}$ bar and C/O = 1.2, carbon abundance enhanced) in order to illustrate fractionations among the highly refractory and refractory REE and actinides.
[b] The range in percentage condensed corresponds to the uncertainties in the thermodynamic data for the condensation reactions.
[c] At $P = 10^{-3}$ bar, GdS condenses as pure sulfide prior to oldhamite at 1418 K.

tainties are always associated with reaction (12) and range from 23.6 kJ/mole for Eu to 77.7 kJ/mole for Yb at 1378.6 K. We therefore used the uncertainties for reaction (12) to calculate the uncertainties given in Fig. 2.

Figure 2 and Table 6 show that except for Sm, Eu, Tm, and Yb, the REE are so refractory that they are fully condensed into oldhamite almost as soon as it forms. This implies that in a gas with a high C/O ratio any ultrarefractory condensates would be much less fractionated than their more oxidized counterparts found in Ornans and other carbonaceous chondrites [5,60]. Assuming condensation of the actinides as sulfides and neglecting other possible prior condensates, Th and U are also fully condensed into oldhamite as soon as it forms and the same is also true for Pu within the uncertainties of the thermodynamic data. We classified the REE and actinides into three categories based on their volatility and condensation behavior at high C/O ratios.

(1) Highly refractory elements

At 10^{-3} bar, the most refractory REE are Gd, Tb, and Lu, which are fully condensed at 0.1 K below the condensation temperature of oldhamite. As shown in Table 6, their fractions condensed are in the range of 99.5 to 100.0% and their gas/solid distribution coefficients range from 0.0004 to 0.002. Their major gases at the oldhamite condensation point are the monosulfides. At 10^{-3} bar pure GdS condenses at 1418 K. At lower pressures pure TbS and LuS also condense prior to CaS (see Table 5).

(2) Refractory elements

The light REE, Dy, Ho, Er, U, and Th are also almost fully condensed at 0.1 K below the condensation temperature of oldhamite by forming solid solutions. These elements have 50% condensation temperatures > 1378 K. However, they are clearly less refractory than the group above because of their smaller fractions condensed and larger gas/solid distribution coefficients. Table 6 also shows that the uncertainties in the thermodynamic data generally lead to small errors, usually only a few percent in the fraction condensed. The exceptions are Ho and Dy where uncertainties in the fractions condensed range from 45 to 93% (Ho) and 20 to 82% (Dy). The most abundant compounds in the gas phase are the monoxides for the light REE (La–Nd), and the monatomic gases for Dy, Ho, and Er. The more refractory behavior of Ce and U at C/O = 1.2 is in contrast to their more volatile behavior in a solar gas. Only Th is mainly present as the dioxide gas at the condensation temperature of oldhamite.

(3) Volatile elements

Sm, Eu, Tm, and Yb fractionate strongly from the other REE because of their greater volatility under these highly reducing conditions, with Yb and Eu being the most volatile REE (see Table 6). Plutonium is slightly more volatile than U or Th. The elements in this category have 50% condensation temperatures below that of oldhamite, however, the 50% condensation temperatures of Tm (1376 K) and Pu (1378) are still very close to the oldhamite condensation temperature (1379 K). There are two reasons for including Tm and Pu in this category. First, the fractions condensed for Tm and Pu are lower than those of any element in the refractory group (although there is some overlap between the upper limit for Pu and the lower limit for Dy). Second, Tm and Pu have gas/solid distribution coefficients larger than any of the refractory elements (although Pu is again closer to Dy than any other element in the volatile group). Whereas the refractory elements are about 50–100% condensed at this temperature, the more volatile elements are < 20%

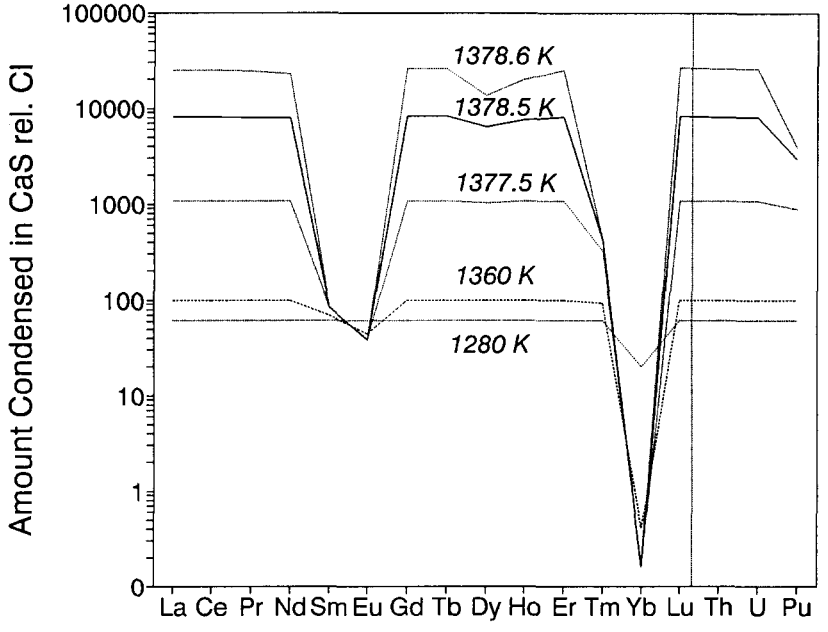

Fig. 3. Predicted REE and actinide enrichments in CaS as a function of condensation temperature at 10^{-3} bar and C/O = 1.2 (carbon abundance increased). The enrichment factors are normalized to CI-chondrite abundances [20]. Note that enrichments of about 100 times CI-chondritic, which have been reported by Larimer and Ganapathy [11] and by Lundberg et al. [13] correspond to condensation at temperatures of about 1360 K. The much higher enrichments of 10,000 times CI-chondritic, which are predicted for REE condensation into CaS as soon as it forms have not yet been reported in meteoritic samples. This ultrarefractory component is analogous to the ultrarefractory component found in Ornans [60] which has REE enrichments of about 10,000 times CI-chondrite for some refractory lithophiles (Lu, Er) and some refractory siderophiles (Ir, Re, Os).

condensed (see Fig. 2 and Table 6). A third distinction is that all of the volatile elements are mainly present in the gas phase as monatomic gases.

Predicted REE and actinide abundance patterns in oldhamite

Calcium condensation starts when oldhamite forms at 1379 K and continues to 1280 K, when all Ca is in CaS. The calculated fraction of Ca condensed was combined with the REE and actinide condensation calculations to predict the CI-chondrite normalized REE and actinide concentrations in oldhamite grains isolated from the nebular gas at different temperatures (Fig. 3).

At 1378.6 K, 0.1 K below the oldhamite condensation point, 0.28% of all Ca is condensed as CaS and condensation of the refractory REE results in an enrichment of about 22,000 times the CI-chondritic abundances. The REE pattern shows significant depletions in Yb, Eu, Sm, and Tm. Plutonium is also depleted relative to Th and U. When the temperature drops to 1377.5 K, where about 6% of total Ca is condensed, the overall shape of the pattern remains the same. However, the enrichments of the refractory REE are lowered to around 1000 times CI because of dilution from the additional CaS. The Eu and Yb enrichment factors are about 50 times CI and about 0.6 times CI, respectively. At 1360 K, about 20 K below the oldhamite condensation point, ~ 60% of all Ca is condensed, further diluting the refractory REE abundances to 100 times CI. There is almost complete condensation of Sm and Eu into oldhamite at this point. The oldhamite REE pattern is basically flat and displays a Yb depletion accompanied by a much smaller Eu depletion. At about 1280 K all Ca is condensed as CaS and the REE abundance in oldhamite is about 62 times CI. Complete condensation of Yb into oldhamite finally takes place at about 1200 K. This is over 100 K above the temperature where anorthite and diopside are predicted to form by reaction of oldhamite with a carbon-rich nebular gas.

Five basic types of REE patterns are predicted by the condensation calculations at high C/O ratios. These patterns are listed below along with the analogous REE patterns in CAIs [5].

(1) Otherwise flat patterns with Yb and Eu depletions. These can be produced by removing oldhamite from equilibrium with the gas at high temperatures. This pattern is analogous to the Group III pattern in CAIs.

(2) Otherwise flat patterns with only a Yb depletion. These are produced by removing an oldhamite grain from equilibrium with the gas at high temperatures where Eu is fully condensed into oldhamite but the more volatile Yb is not. There is no analogous REE pattern in CAIs.

(3) Flat REE patterns in oldhamite grains which equilibrated with the nebular gas down to temperatures where all REE condensed out. The temperature required for full condensation of all REE into oldhamite is about 100 K higher than the temperature where oldhamite will react to form diopside or anorthite. The analogous pattern in CAIs is the Group V pattern.

(4) and (5) Complementary patterns to the first two cases. These patterns have either Yb excesses, or Eu and Yb excesses, like the analogous Group VI pattern in CAIs. These patterns result when Eu and Yb remaining in the gas (after condensation of the more refractory REE) condense into REE-bearing oldhamites with flat patterns. This occurs by mixing gas and grains from different nebular reservoirs. This model is directly analogous to that discussed for producing the Group VI patterns in CAIs [61].

Comparison of predicted and observed REE patterns

The published REE patterns in oldhamites from primitive enstatite chondrites (EH3/4) fall into three categories: (1) relatively unfractionated flat patterns, (2) relatively unfractionated flat patterns with Yb excesses, and (3) relatively unfractionated flat patterns with both Yb and Eu excesses (patterns A to D of Lundberg et al. [13]). However, no patterns with Yb depletions or with Yb and Eu depletions have been observed. All of the observed patterns can be explained by REE condensation into oldhamite and subsequent removal of the CaS grains from equilibrium with the nebular gas.

The unfractionated pattern "A" with LREE abundances about 80–90 times CI and HREE abundances of about 60 times CI can be pro-

duced by equilibration of an oldhamite grain with the nebular gas down to temperatures where the REE are completely condensed (case 3 above). A.M. Davis [pers. commun., 1992] suggests that the apparent LREE enrichment in pattern "A" may be an artifact due to the use of perovskite standards and sensitivity factors for ion probe analyses of REE in sulfides coupled with possible systematic differences between oxide and sulfide ion yields that vary smoothly with atomic number. If this is so, then the match between the observed pattern "A" and the predicted case (3) is improved. Oldhamites displaying patterns with either Yb or Yb and Eu excesses, and abundances of 70–40 times CI for the LREE to HREE (patterns "B" and "C" of Lundberg et al. [13]) fall into our categories (4) and (5) above. They are probably CaS grains which formed at a low temperature where all the REE in one nebular reservoir completely condensed into oldhamite. The Yb or Yb and Eu excesses result when additional Yb or Yb and Eu from another nebular reservoir condense into the grains with flat patterns. Either gas or grain transport can cause this. This process is analogous to that postulated for the origin of the Group VI and Group I REE patterns in CAIs. The type "D" pattern is an extreme example of cases (4) and (5) discussed above. The slightly higher Sm and Tm enrichments relative to the other REE are due to their slightly greater volatility (Table 5). The match between the observed pattern "D" and the predicted patterns (4) and (5) would improve if the LREE abundance trend were an artifact as suggested by Davis (see above).

Lundberg and coworkers also report patterns displaying REE enrichment factors of about 500 times CI with Eu depletions often accompanied by Yb excesses (pattern "E"). However, this type of pattern is only observed in weathered samples from the Antarctic. The high REE enrichments may be artifacts, because the reported REE pattern is based on measured REE/Ca ratios and the assumption that the phase analyzed is stoichiometric oldhamite. Solubility studies show that Ca is more likely to be removed from oldhamite by aqueous weathering than the REE [62]. Therefore, Ca removal would cause a relative enrichment of the REE. Aqueous weathering can also easily account for the observed Eu depletion in Type "E" oldhamites because Eu is the most leachable of the REE elements from aubrites and certainly also from enstatite chondrites [62]. For example, Lodders and Palme [62] showed that a water leach removes about 20% of total Ca, 13% of total Eu, and $< 5\%$ of total Yb and Lu from the Peña Blanca Spring aubrite, while the other REE require more acidic solvents to be leached. Based on leaching studies of the REE and Ca from enstatite chondrites [6], Sears et al. [16] also concluded that Ca is probably more easily leached from oldhamite than are the REE. On the other hand, Floss et al. [63] measured a suite of similar REE patterns in weathered and unweathered oldhamites in the Bishopville and Bustee aubrites. Based on these data they argued that terrestrial weathering effects will not alter fractionated REE abundance patterns in meteoritic oldhamites. However, without knowing whether or not the weathering took place in the presence of liquid water, which presumably could remove the more easily leachable REE, or only in the presence of atmospheric water vapor, which presumably could not remove any non-volatile elements, it is difficult to determine if the conclusions of Floss et al. [63] are in conflict with the results of the experimental leaching studies of Shima and Honda [6] and Lodders and Palme [62].

In addition to the REE patterns described above, oldhamite in more equilibrated enstatite chondrites (EL6) displays REE enrichments about 100 times CI, except for Eu which is enriched only 20 times CI [12]. From our calculations it is apparent that an Eu depletion will always be accompanied by a Yb depletion, if the observed pattern is solely due to nebular condensation. However, in these samples, Yb is as enriched as the other HREE. The large enrichments of the refractory REE and Yb suggest that all the REE condensed fully into oldhamite and then, later on, thermal metamorphism led to a redistribution of Eu. Since albitic plagioclase is a major constituent of enstatite chondrites [64] and Eu shows preferential partitioning into plagioclase, Eu loss from oldhamite is easily envisioned. Thus we suggest that the REE patterns characterized by Eu depletions are due to thermal metamorphism.

Larimer and Ganapathy [11] reported neutron activation analyses for some of the REE in oldhamites from a chondrule in Indarch (EH4) and

from the matrix in Yilmia (EL6). However, because of the generally small sample sizes, they were only able to obtain partial REE patterns. Both samples display relatively unfractionated REE patterns with LREE abundances about 100–300 times CI and the HREE abundances about 30–40 times CI. The reported pattern in Indarch is broadly consistent with other analyses of oldhamites in Indarch [12]. Both patterns probably formed by complete or almost complete REE condensation into oldhamite at low temperatures (about 1280 K at 10^{-3} bar total pressure). The high concentrations of volatile Cs, Sb, and Zn in these oldhamites indicate vapor–solid equilibrium down to even lower temperatures because these volatile elements will not condense until after all REE are out of the gas [11].

Uranium and Th in oldhamite from primitive and more equilibrated enstatite chondrites are enriched 30–50 times CI [8,14]. Murrell and Burnett [14] also found essentially unfractionated Th/U ratios ranging from ~ 3.5 (in Abee, EH4) to ~ 4.2 (in St. Mark's, EL5). These results are consistent with the calculations illustrated in Fig. 3 which predict actinide enrichments of about 60 times CI-chondritic in CaS at 1280 K and unfractionated Th/U ratios in oldhamites formed below about 1377 K, if both Th and U condensed into CaS. As mentioned earlier, Th is predicted to condense as ThN over the 10^{-3} to 10^{-9} bar pressure range and U is predicted to condense as UC at pressures $\leqslant 10^{-6}$ bar. However, at 10^{-2} bar there is only a 10 K difference between the ThN and ThS (dissolved in CaS) condensation temperatures. This small interval is within the uncertainties of the thermodynamic data for ThS and ThN and thus it is possible that ThS will actually condense at this pressure. Even if this does not occur, the similar crystal structures of ThN and CaS will probably lead to mutual solid solution.

The origin of oldhamite in enstatite chondrites

Up to this point we have implicitly assumed that the REE-rich oldhamites found in enstatite chondrites formed by condensation from an otherwise solar gas with an enhanced C/O ratio. This assumption is shared by other workers [e.g., 11]. However, it is also possible that at least some of the oldhamite grains in enstatite chondrites may have formed by the sulfurization of pre-existing Ca-bearing solids in the solar nebula or by metamorphic reactions on the meteorite parent body. However, we will show that condensation of oldhamite at enhanced C/O ratios in the solar nebula is the most plausible origin of the REE-rich oldhamites found in enstatite chondrites.

Arguments against oldhamite formation by sulfurization reactions in the solar nebula

Larimer's calculations [1,2] showed that a new suite of reduced carbide, nitride, and sulfide minerals appears in the condensation sequence as the C/O ratio is increased from the solar value to values of one and above. Initially these minerals form by the reduction of pre-existing oxide and silicate phases, but later as the C/O ratio increases to unity, they become the initial condensates. In the case of CaS, there are several possible routes for forming it from pre-existing Ca-bearing phases in the solar nebula at the intermediate C/O ratios where CaS is stable but is not an initial condensate.

Larimer et al. [2,11] noted that CaS could be formed from perovskite by the reaction:

$$CaTiO_3 + H_2S(g) + \tfrac{1}{2}N_2(g) + 2H_2(g) = CaS + TiN + 3H_2O(g) \quad (13)$$

or be produced from diopside via the reaction:

$$CaMgSi_2O_6 + H_2S(g) + Mg(g) = CaS + 2MgSiO_3 + H_2(g) \quad (14)$$

The former reaction can only form a few percent of the total oldhamite found in enstatite chondrites because of the small Ti/Ca solar abundance ratio of about 4 atom% [11]. Furthermore, we find that N_2 fugacities of ~ 0.01 bar are required for this reaction. This is about 10^5 times larger than the N_2 fugacity at 10^{-3} bar pressure in the solar nebula. Likewise reactions forming CaS and TiC from perovskite or CaS and AlN from hibonite are also thermodynamically unfavorable under nebular conditions because of the high CO or N_2 fugacities involved. These reactions are probably also kinetically inhibited because they involve breaking either the N_2 triple

bond to form TiN or AlN or involve breaking the CO triple bond to form TiC.

Reaction (14), the sulfurization of diopside to CaS and enstatite is thermodynamically favorable within the enstatite stability field. However, this reaction cannot produce REE-rich oldhamite for two reasons: (1) all the REE have already condensed into perovskite or hibonite well above the temperature at which oldhamite is predicted to form by diopside sulfurization, and (2) diopside is not a favorable REE host phase.

We also considered fassaite which is the major REE host phase in some Type B CAIs [65]. No thermodynamic data are available for fassaite and thus it is not possible to calculate whether or not it is a condensate or if fassaite will actually convert to oldhamite under high C/O ratios in the solar nebula. The REE patterns in fassaites studied by Simon et al. [65] are characterized by large Eu depletions and increasing enrichments from the LREE to HREE. However, these patterns have not been found in oldhamites in enstatite chondrites and therefore derivation of these oldhamites from pre-existing fassaite is unlikely.

If REE-rich oldhamite were produced by the sulfurization of perovskite or hibonite, the secondary oldhamite would inherit the REE pattern of the original host phase. As noted above, oldhamite production from these phases is thermodynamically implausible. Nevertheless, we investigated whether or not any of the REE patterns observed in oldhamite could have been produced by REE condensation into perovskite or hibonite, followed by sulfurization of these phases to form CaS. We calculated the 50% condensation temperatures of the REE at C/O ratios of 0.9–1.0, where perovskite and hibonite form prior to CaS. The resulting REE patterns have small Ce depletions and larger, approximately equal sized Eu and Yb depletions. These patterns are unlike those reported in oldhamites in enstatite chondrites.

Alternatively, oldhamite may have formed by the sulfurization of whole CAIs or chondrules. In the former case, assemblages composed of oldhamite, niningerite, quartz, and corundum are predicted. These are not observed in enstatite chondrites. In the latter case, the REE in the chondrule will be divided between the niningerite and oldhamite which form from the sulfurization. Also, low REE enrichments of only a few times chondritic in the niningerite and oldhamite, corresponding to the generally low enrichments of REE in chondrules will probably be found. Therefore, these alternatives are also implausible.

Arguments against oldhamite formation by metamorphic reactions on meteorite parent bodies

It is very unlikely that oldhamite formed by metamorphic reactions on a meteorite parent body [11]. Oldhamite formation by metamorphism requires the reduction of Ca-bearing oxides and/or silicates. This reaction is driven toward CaS by either a high sulfur fugacity or a low oxygen fugacity. However, the sulfur fugacity in both the ordinary and enstatite chondrite parent bodies was probably buffered by Fe–FeS. Thus the driving force for CaS formation must be the low oxygen fugacity and not the high sulfur fugacity [11]. Otherwise, CaS would also be found in ordinary chondrites, which is not the case. But an oxygen fugacity low enough to reduce CaO (in an oxide or silicate phase) to CaS will also easily reduce Mg and Si. Although a small fraction of Mg and Si are present in reduced form (e.g., MgS, Si in metallic Fe) they are dominantly ($> 90\%$) present as $MgSiO_3$.

The possible formation of CaS by metamorphic reactions is also contradicted by the work of Petaev [66] who showed the lack of any statistically significant correlation between the CaS abundance and metamorphic type. If CaS were formed during metamorphism, its abundance would be expected to be higher in the more metamorphosed and more equilibrated EL6 chondrites. However, this is not the case.

The high REE enrichments found in oldhamite present another problem. Oldhamite is present at about the 1% level in enstatite chondrites, yet it contains all, or nearly all, of the REE in these meteorites. If the CaS were a secondary phase formed on the parent body, a process to efficiently remove all the REE from all other host phases and to concentrate the REE into oldhamite has to be postulated. In this case the original REE host phase is presumably another refractory mineral such as perovskite or hibonite. The survival of these minerals in CAIs

is due to their ability to withstand destructive chemical reactions in the hot (> 1500 K) nebular gas. If these minerals can withstand attack by the hot, corrosive nebular gas, then it is unlikely that they will react away during the much milder temperatures experienced during metamorphism on meteorite parent bodies.

Finally, the analytical results of Larimer and Ganapathy [11] also argue against metamorphic incorporation of the REE into oldhamite. They found that the REE were more enriched in CaS from Indarch, a primitive EH4 chondrite, than in CaS from Yilmia, a more equilibrated EL6 chondrite. The decreasing abundance of Mg and the increasing abundance of Mn in the two oldhamite samples also followed the trend observed in going from low to high petrologic type [64]. This is the opposite of what would be expected if metamorphic reactions were responsible for incorporating the REE into oldhamites in enstatite chondrites. Thus, the available analytical data and fundamental theoretical considerations argue against a metamorphic origin for REE-rich oldhamites in enstatite chondrites.

Oldhamite condensation at high C / O ratios in the solar nebula

The arguments discussed above strongly suggest that oldhamite in enstatite chondrites did not form by the reactions of pre-existing condensates with nebular vapor or by metamorphic reactions on meteorite parent bodies. Instead, the most plausible origin for the REE-rich oldhamites found in enstatite chondrites is condensation at high C/O ratios in the solar nebula [1–3,11].

There are basically two ways to increase the C/O ratio of nebular gas above the solar value: by removing oxygen or by adding carbon. Mass balance dictates that to a good first approximation, most of the oxygen in the nebular gas was in the form of H_2O (~ 58%) and CO (~ 42%). Other gaseous species such as OH and O only become important at higher temperatures above the condensation point of CaS, while the thermodynamically favorable conversion of CO to CH_4 at lower temperatures is kinetically inhibited over the lifetime of the solar nebula [67,68]. Once appreciable amounts of silicates such as enstatite condense, about 13% of the total oxygen is tied up in rocky material and thus increases the C/O ratio in the nebular gas. However, the resulting increase is small (C/O increases from ~ 0.42 to ~ 0.46), and it does not take place until silicate condensation occurs at temperatures below the formation point of graphite, SiC, TiC, and many of the other unusual minerals. Thus, another process is necessary if large amounts of oxygen are to be removed from the nebular gas.

One possible process is condensation of water ice [69]. Stevenson and Lunine [70] recently modelled the diffusive redistribution of water vapor in the solar nebula while nebular gas was still present. They calculated profiles showing the water vapor abundance as a function of time and distance (R) in the inner solar nebula ($R \leqslant 5$ A.U.). As noted by Fegley and Prinn [68], desiccation of the inner solar nebula leads to high C/O ratios in the gas phase. Oldhamite and the other reduced minerals found in enstatite chondrites can then form. Depending on the timing of the diffusive transport of H_2O(g) more or less enstatite chondrite-like material can be produced in the inner solar nebula. In fact, enstatite chondrites make up only ~ 1% (by number, less by mass) of all chondrites in museum collections, so the diffusive transport process could have occurred relatively late during the nebular lifetime.

An alternative mechanism to increase the C/O ratio is the vaporization of carbonaceous dust [2,3,11]. This suggestion is supported by the discovery of interstellar graphite and SiC grains in chondrites [71,72]. Interstellar carbonaceous dust was definitely present in the solar nebula and some small fraction survived vaporization and destruction in the nebular gas. However, the amounts of interstellar SiC and graphite found, typically a few ppm to a few tens of ppm by mass, are substantially lower than the estimated mass fractions of ~ 14% (for graphite) to ~ 39% (for graphite + amorphous carbon + polyaromatic hydrocarbons (PAHs) + organic refractories) for the different types of carbonaceous dust ejected into the interstellar medium at the present time [73]. Assuming a similar abundance of carbonaceous material in interstellar dust 4.56 billion years ago, this discrepancy suggests that the amount of carbonaceous dust accreted by the solar nebula may have been much larger than the amounts presently

observed in primitive meteorites. If so, then the vaporization of large amounts of carbonaceous dust may have produced nebular regions having enhanced C/O ratios. In any case, the evidence for the postulated vaporization of carbonaceous dust in the solar nebula is now stronger than it was prior to the discovery of interstellar SiC and graphite in meteorites.

Finally, we consider oldhamite formation by an evaporative process in the solar nebula. For example, the nucleosynthetic isotopic anomalies in Ca and Ti in some hibonite grains from CM2 chondrites suggest that these CAIs are evaporative residues [5]. If these inclusions had been formed by condensation, then the nucleosynthetic anomalies would not be present because the Ca and Ti isotopes would have been homogenized in the nebular gas prior to condensing out as a hibonite grain. However, the few available data on the Ca isotopic composition of oldhamites show δ^{48}Ca values ranging from -3 to $-7‰$ [13], which are about an order of magnitude smaller than the ^{48}Ca nucleosynthetic anomalies (both positive and negative) observed in the CM2 hibonites. The smaller isotopic anomalies in the oldhamites do not provide as strong a motivation for proposing an evaporative origin of the oldhamites in which they occur.

Conclusions

We calculated REE and actinide condensation into oldhamite (CaS), which is the major REE and actinide host phase in the highly reduced enstatite chondrites. The major results are:

(1) We confirm the trends reported by Larimer et al. [1,2] for the cosmochemical behavior of the major elements as a function of C/O ratio in an otherwise solar gas. Oxide and silicate condensation temperatures decrease with increasing C/O ratio, dropping sharply at C/O ratios > 0.9. At C/O ratios $\geqslant 1$, carbides, nitrides, and sulfides replace oxides and silicates as the initial condensates of the major elements.

(2) We find that most of the REE, Th, U, and Pu condense fully into oldhamite as soon as it condenses. This occurs at about 1379 K for a C/O ratio of 1.2 and a total pressure of 10^{-3} bar. The exceptions are Yb and Eu, which are the most volatile REE under these highly reducing conditions. Ce is as refractory as the other LREE. This is in contrast to a solar gas, where Ce is more volatile than the LREE and many other refractory lithophiles [4].

(3) The pressure dependence of REE and actinide condensation into oldhamite over the 10^{-3} to 10^{-9} bar range was compared to REE and actinide condensation in a solar gas over the same pressure range. At the same total pressure, perovskite and hibonite, two major REE and actinide host phases in CAIs, condense at temperatures about 310 to 370 K higher than CaS does. As a consequence of this, the REE and actinides have lower 50% condensation temperatures at C/O = 1.2 than at the solar C/O ratio of 0.42. Furthermore, REE patterns formed at high C/O ratios are much less fractionated than their counterparts formed in a solar gas.

(4) Five basic types of REE abundance patterns in oldhamite formed at high C/O ratios are predicted: (i) Otherwise flat patterns with depletions in Yb and Eu. (ii) Otherwise flat patterns with only a Yb depletion. (iii) Flat REE patterns in oldhamite grains which equilibrated with the nebular gas down to temperatures where all REE condensed out. The temperature required for full condensation of all REE into oldhamite is about 100 K higher than the temperature where oldhamite will react to form diopside or anorthite. (iv) and (v) Complementary patterns to the first two cases. These patterns exhibit either Yb excesses, or Eu and Yb excesses.

(5) A comparison of the predicted REE patterns and the observed patterns reported in the literature [11–13] shows that all of the observed patterns can be explained in terms of condensation at high C/O ratio in an otherwise solar gas. The observed patterns fall into 3 of the 5 categories listed above. No patterns which match the first two types (i.e., those with either Yb and Eu or only Yb depletions) have been reported in the literature.

(6) The observed Th and U enrichments and ratios in oldhamites from enstatite chondrites are also consistent with our condensation calculations at high pressures of about 10^{-2} bar. At lower pressures the predicted condensation of Th as ThN and of U as either US in CaS or as pure UC may lead to Th/U fractionations. The lack of such fractionations in enstatite chondrites may

indicate either condensation at the relatively high pressure of 10^{-2} bar or solid solution of the isostructural (NaCl) ThN, US, and UC phases formed at lower pressures. The lack of data on the phase diagrams of these species and on diffusion coefficients for Th and U in these phases precludes more definitive predictions at this time.

(7) We and others [11] present evidence showing that condensation from an otherwise solar gas with a C/O ratio $\geqslant 1$ is the most plausible origin for the REE-rich oldhamites found in enstatite chondrites. Thus, careful study of the trace element patterns in oldhamite and in the other unusual minerals found in the enstatite chondrites has the potential to provide constraints on the chemical and physical conditions in the region of the solar nebula where these meteorites formed.

Acknowledgements

B.F. acknowledges support by grants from the NASA Planetary Atmospheres and Origins of Solar Systems Programs. During revision of the paper K.L. was partially supported by these grants. The CONDOR code was developed by CRD and C.

References

1 J.W. Larimer, The effect of C/O ratio on the condensation of planetary material, Geochim. Cosmochim. Acta 39, 389–392, 1975.
2 J.W. Larimer and M. Bartholomay, The role of carbon and oxygen in cosmic gases: some applications to the chemistry and mineralogy of enstatite chondrites, Geochim. Cosmochim. Acta 43, 1453–1466, 1979.
3 J.W. Larimer, An experimental investigation of oldhamite, CaS; and the petrologic significance of oldhamite in meteorites, Geochim. Cosmochim. Acta 32, 965–982, 1968.
4 A. Kornacki and B. Fegley, The abundance and relative volatility of refractory trace elements in Allende Ca, Al-rich inclusions: Implications for chemical and physical processes in the solar nebula, Earth Planet. Sci. Lett. 79, 217–234, 1986.
5 B. Fegley Jr. and T.R. Ireland, Chemistry of the rare earth elements in the solar nebula, Eur. J. Solid State Inorg. Chem. 28, 335–346, 1991.
6 M. Shima and M. Honda, Distributions of alkali, alkaline earths and rare earth elements in component minerals of chondrites, Geochim. Cosmochim. Acta 31, 1995–2006, 1967.
7 R.M. Frazier and W.V. Boynton, Rare earth and other elements in components of the Abee enstatite chondrite, Meteoritics 20, 197–218, 1985.
8 M.J. Furst, M.I. Stapanian and D.S. Burnett, Observations of non-lithophile behavior for U, Geophys. Res. Lett. 9, 41–44, 1982.
9 Y. Zhang, P.H. Benoit and D.W.G. Sears, The thermal history of enstatite chondrites (abstr.), Meteoritics 27, 310–311, 1992.
10 J.W. Larimer and R. Ganapathy, Trace element content of oldhamite and other minerals unique to enstatite chondrites (abstr.), Meteoritics 18, 334, 1983.
11 J.W. Larimer and R. Ganapathy, The trace element chemistry of CaS in enstatite chondrites and some implications regarding its origin, Earth Planet. Sci. Lett. 84, 123–134, 1987.
12 L.L. Lundberg and G. Crozaz, Enstatite chondrites: A preliminary ion microprobe study (abstr.), Meteoritics 23, 285–286, 1988.
13 L.L. Lundberg, G. Crozaz and E. Zinner, Ca and S isotopic compositions and REE concentrations in oldhamite of five unequilibrated enstatite chondrites (abstr.), Lunar Planet. Sci. Conf. XXII, pp. 835–836, 1991.
14 M.T. Murrell and D.S. Burnett, Actinide microdistributions in the enstatite meteorites, Geochim. Cosmochim. Acta 46, 2453–2460, 1982.
15 B. Fegley Jr., Chemical fractionations in enstatite chondrites (abstr.), Meteoritics 17, 210–212, 1982.
16 D.W. Sears, G.W. Kallemeyn and J.T. Wasson, Composition and origin of clasts and inclusions in the Abee enstatite chondrite breccia, Earth Planet. Sci. Lett. 62, 180–192, 1983.
17 J.W. Larimer, H.A. Bartholomay and B. Fegley, The chemistry of rare earth elements in the solar nebula (abstr.), Meteoritics 19, 258, 1984.
18 S.S. Barshay and J.S. Lewis, Chemical structure of the deep atmosphere of Jupiter, Icarus 33, 593–611, 1978.
19 B. Fegley Jr. and H. Palme, Evidence for oxidizing conditions in the solar nebula from Mo and W depletions in refractory inclusions in carbonaceous chondrites, Earth Planet. Sci. Lett. 72, 297–310, 1985.
20 E. Anders and N. Grevesse, Abundances of the elements: Meteoritic and solar, Geochim. Cosmochim. Acta 53, 197–214, 1989.
21 T.V. Charlu, R.C. Newton and O.J. Kleppa, Thermochemistry of synthetic $Ca_2Al_2SiO_7$ (gehlenite)–$Ca_2MgSi_2O_7$ (akermanite) melilites, Geochim. Cosmochim. Acta 45, 1609–1617, 1981.
22 D.R. Waldbaum, The configurational entropies of $Ca_2Al_2SiO_7$–$Ca_2MgSi_2O_7$ melilites and related minerals, Contrib. Mineral. Petrol. 39, 33–54, 1973.
23 J.H. Jones, The geochemical coherence of Pu and Nd and the $^{244}Pu/^{238}U$ ratio of the early solar system, Geochim. Cosmochim. Acta 46, 1793–1804, 1982.
24 N. Grevesse, D.L. Lambert., A.J. Sauval, E.F. van Dishoeck, C.B. Farmer and R.H. Norton, Vibration-rotation bands of CH in the solar infrared spectrum and the solar carbon abundance, Astron. Astrophys. 242, 488–495, 1991.
25 A.G.W. Cameron, Elementary and nuclidic abundances in the solar system, in: Essays in Nuclear Astrophysics, C.A. Barnes, D.D. Clayton and D.N. Schramm, eds., pp. 23–43, Cambridge Univ. Press, 1982.

26 J.M. Lattimer and L. Grossman, Chemical condensation sequences in supernova ejecta, Moon Planets 19, 169–184, 1978.
27 M.W. Chase Jr., C.A. Davies, J.R. Downey Jr., D.J. Frurip, R.A. McDonal and A.N. Syverud, JANAF Thermochemical Tables, 3rd. ed., J. Phys. Chem. Ref. Data 14, suppl. No. 1, 1985.
28 B.S. Hemingway, J.L. Haas Jr., and G.R. Robinson Jr., Thermodynamic properties of selected minerals in the system Al_2O_3–CaO–SiO_2–H_2O at 298.15 K and 1 Bar (10^5 Pascals) pressure and at higher temperatures, US Geol. Surv. Bull. 1544, 70 pp., 1982.
29 R. Hultgren, P.D. Desai, D.T. Hawkins, M. Gleiser, K.K. Kelley and D.D. Wagman, Selected values of the thermodynamic properties of the elements, 636 pp., Am. Soc. Metals, Metals Park, OH, 1973.
30 K.C. Mills, Thermodynamic Data for Inorganic Sulphides, Selenides and Tellurides, 845 pp., Butterworths, London, 1974.
31 L.B. Pankratz, Thermodynamic properties of elements and oxides, US Bur. Mines Bull. 672, 509 pp., 1982.
32 L.B. Pankratz, Thermodynamic properties of halides, US Bur. Mines Bull. 674, 826 pp., 1984.
33 L.B. Pankratz, J.M. Stuve and N.A. Gokcen, Thermodynamic data for mineral technology, US Bur. Mines Bull. 677, 355 pp., 1984.
34 L.B. Pankratz, A.D. Mah and S.W. Watson, Thermodynamic properties of sulfides, US Bur. Mines Bull. 689, 472 pp., 1987.
35 R.A. Robie, B.S. Hemingway and J.R. Fisher, Thermodynamic properties of minerals and related substances at 298.15 K and 1 bar (10^5 Pascals) pressure and at higher temperatures, Geol. Surv. Bull. 1452, 456 pp., 1979.
36 R.J. Ackermann and M.S. Chandrasekharaiah, Systematic thermodynamic properties of actinide metal–oxygen systems at high temperatures, in: Thermodynamics of Nuclear Materials Vol. II, pp. 3–26, Int. Atomic Energy Agency, Vienna, 1975.
37 C.E. Holley, M.H. Rand and E.K. Storms, The chemical thermodynamics of actinide elements and compounds, Part 6. The actinide carbides, 101 pp., Int. Atomic Energy Agency, Vienna, 1984.
38 E. Murad and D.L. Hildenbrand, Dissociation energies of GdO, HoO, ErO, TmO, and LuO; correlation of results for the lanthanide monoxide series, J. Chem. Phys. 73, 4005–4011, 1980.
39 M.A. Mignanelli, P.E. Potter and M.H. Rand, The phase relationships and thermochemical properties of the cerium–oxygen system, a critical assessment, 38 pp., Comm. Eur. Commun. Rep. EUR 7820, 1982.
40 C.E. Myers and D.T. Graves, Thermodynamic properties of lanthanide trihalide molecules, J. Chem. Eng. Data 22, 436–439, 1977.
41 M.H. Rand, Thermochemical properties, in: Thorium: Physico-chemical Properties of its Compounds and Alloys, O. Kubaschewski ed., pp. 7–86, Int. Atomic Energy Agency, Vienna, 1975.
42 R.C. Brown and N.J. Clark, Knudsen cell vaporization of rare earth nitrides: Enthalpy of vaporization of $HoN_{0.98}$, High Temp. Sci. 7, 131–141, 1975.
43 R.C. Brown and N.J. Clark, Knudsen cell vaporization of rare earth nitrides: Enthalpy of vaporization of SmN and YbN, High Temp. Sci. 10, 71–84, 1978.
44 V.P. Glushko, L.V. Gurvich, G.A. Bergman, I.V. Veitz, V.A. Medvedev, G.A. Khachcurvzov, V.S. Yungman, eds., Thermodynamic Properties of Individual Substances, Parts 1–4, High Temperature Inst., Moscow, 1978–1982.
45 J.M. Haschke and T.A. Deline, Vaporization and thermodynamic properties of samarium dicarbide and substoichiometric disamarium tricarbide, J. Chem. Thermodyn. 14, 1019–1028, 1978.
46 O. Kubaschewski and C.B. Alcock, Metallurgical Thermochemistry, 183 pp., 5th ed., Pergamon, New York, NY, 1979.
47 K.A. Gschneidner and N. Kippenhan, Thermochemistry of the rare earth carbides, nitrides and sulfides for steelmaking, 25 pp., Rare Earth Inf. Cent., Ames, IA, Rep. IS-RIC-5, 1971.
48 F. Gronvold, J. Drowart, and E.F. Westrum Jr., The chemical thermodynamics of actinide elements and compounds. Part 4. The actinide chalcogenides (Excluding oxides), 265 pp., Int. Atomic Energy Agency, Vienna, 1984.
49 E.D. Cater and R.P. Steiger, Vaporization, thermodynamics, and dissociation energy of lanthanum monosulfide. II, J. Phys. Chem. 78, 2231–2233, 1968.
50 L.N. Vasilev, V.M. Grabov, A.V. Golubkov, A.G. Gorobets, V.S. Oskotskii, I.A., Smirnov, and V.V. Tikhonov, Physical properties and phase transitions of the rare earth monosulphides in the homogeneity range, Phys. Status Solidi (A) 80, 237–244, 1983.
51 J.A. Fries and D.E. Cater, Vaporisation, thermodynamics, and dissociation energy of gadolinium monosulfide: systematics of vaporisation of the rare earth monosulfides, J. Chem. Phys. 68, 3978–3989, 1978.
52 S. Smoes, J. Drowart and J.M. Welter, Thermodynamic study of the vaporization of europium monosulfide by Knudsen-cell mass spectrometry. Atomization energies of EuS(g), Eu2S(g), EuS2(g), Eu2O(g), Eu2OS(g), and Eu2S2(g), J. Chem. Thermodyn. 9, 275–292, 1977.
53 A.V. Hariharan and H.A. Eick, Vaporisation thermodynamics of europium(II) sulfide, High Temp. Sci. 3, 123–129, 1971.
54 H.F. Franzen and A.V. Hariharan, The high temperature vaporisation and thermodynamics in the lutetium–sulfur system, J. Chem. Phys. 70, 4907–4915, 1979.
55 A. Kornacki and B. Fegley, Origin of spinel-rich chondrules and inclusions in carbonaceous and ordinary chondrites, Proc. 14th. Lunar Planet. Sci. Conf., J. Geophys. Res. 89, B588–B596, 1984.
56 H. Palme and B. Fegley, High temperature condensation of iron-rich olivine in the solar nebula, Earth Planet. Sci. Lett. 101, 180–195, 1990.
57 L. Grossman, C.A. Geiger, O.J. Kleppa, B.O. Mysen and J.M. Lattimer J.M., Stability of hibonite and $CaAl_4O_7$ in the solar nebula, Lunar Planet. Sci. 19, 437–438, 1988.
58 J.B. Pedley and E.M. Marshall, Thermochemical data for gaseous monoxides, J. Phys. Chem. Ref. Data 12, 967–1031, 1983.
59 W.V. Boynton, Fractionation in the solar nebula: conden-

sation of yttrium and the rare earth elements, Geochim. Cosmochim. Acta 39, 569–584, 1975.
60 H. Palme, F. Wlotzka, K. Nagel and A. El Goresy, An ultra-refractory inclusion from the Ornans carbonaceous chondrite, Earth Planet. Sci. Lett. 61, 1–12, 1982.
61 L. Grossman, Refractory inclusions in the Allende meteorite, Ann. Rev. Earth Planet. Sci. 8, 559–608, 1980.
62 K. Lodders and H. Palme, Trace elements in mineral separates of the Pena Blanca Spring aubrite (abstr.), Lunar Planet. Sci. Conf. XXII, pp. 821–822, 1991.
63 C. Floss, M.M. Strait and G. Crozaz, Rare earth elements and the petrogenesis of aubrites. Geochim. Cosmochim. Acta 54, 3553–3558, 1990.
64 K. Keil, Mineralogical and chemical relationships among enstatite chondrites, J. Geophys. Res. 73, 6945–6976, 1968.
65 S.B. Simon, L. Grossman and A.M. Davis, Fassaite composition trends during crystallization of Allende type B refractory inclusion melts, Geochim. Cosmochim. Acta 55, 2635–2655, 1991.
66 M.I. Petaev, Oldhamite as an indicator of disequilibrium during enstatite chondrite accretion (abstr.), Lunar Planet. Sci. Conf. XXII, pp. 1057–1058, 1991.
67 J.S. Lewis and R.G. Prinn, Kinetic inhibition of CO and N_2 reduction in the solar nebula, Astrophys. J., 238, 357–364, 1980.
68 B. Fegley Jr. and R.G. Prinn, Solar nebula chemistry: Implications for volatiles in the solar system, in: The Formation and Evolution of Planetary Systems, H.A. Weaver and L. Danly, eds., pp. 171–211, Cambridge Univ. Press, 1989.
69 P.A. Baedecker and J.T. Wasson, Elemental fractionations among enstatite chondrites, Geochim. Cosmochim. Acta 39, 735–765, 1975.
70 D.J. Stevenson and J.I. Lunine, Rapid formation of Jupiter by diffusive redistribution of water vapor in the solar nebula, Icarus 75, 146–155, 1988.
71 T. Bernatowicz, G. Fraundorf, M. Tang, E. Anders, B. Wopenka, E. Zinner and P. Fraundorf, Evidence for interstellar SiC in the Murray carbonaceous meteorite, Nature 330, 728–730, 1987.
72 S. Amari, E. Anders, A. Virag and E. Zinner, Interstellar graphite in meteorites, Nature 345, 238–240, 1990.
73 A.G.G.M. Tielens and L.J. Allamandola, Composition, structure, and chemistry of interstellar dust, in: Interstellar Processes, D.J. Hollenbach and H.A. Thronson Jr., eds., pp. 397–469, Reidel, Amsterdam, 1987.